Main Manuscript for:

Mobility of nucleosomes is regulated by their binding partners

Daniël P. Melters[1,*]

1 National Cancer Institute, Center for Cancer Research, Laboratory Receptor Biology and Gene Expression, 41 Medlars Drive, Bethesda, MD 20892, USA

Keir C. Neuman[2,*]

2 National Heart, Lung, and Blood Institute, Laboratory of Single Molecule Biophysics, 50 South Drive, Bethesda, MD 20892, USA

Tatini Rakshit[1,3]

1 National Cancer Institute, Center for Cancer Research, Laboratory Receptor Biology and Gene Expression, 41 Medlars Drive, Bethesda, MD 20892, USA

3 Department of Chemistry, Shiv Nadar University, NH91, Dadri, Uttar Pradesh 201314, India

Yamini Dalal[1,*]

1 National Cancer Institute, Center for Cancer Research, Laboratory Receptor Biology and Gene Expression, 41 Medlars Drive, Bethesda, MD 20892, USA

* To whom correspondence should be addressed: Email: dalaly@mail.nih.gov; neumankc@mail.nih.gov; daniel.melters@nih.gov

Author Contributions: D.P.M., K.C.N., T.R., and Y.D. designed research; D.P.M. performed research; D.P.M. and K.C.N. contributed new reagents/analytical tools; D.P.M., K.C.N., and Y.D. analyzed data; D.P.M. and Y.D. wrote the paper.

Competing Interest Statement: The authors declare no competing interest.

Classification: Biological Sciences, Biophysics and Computational Biology

Keyword: epigenetics, nucleosomes, chromatin, chromatin accessibility, high-speed AFM

This PDF contains:

Main text

Figure 1-5

Table 1

Abstract

Chromatin accessibility is modulated in a variety of ways, both to create open and closed chromatin states which are critical for eukaryotic gene regulation. At the mechanistic single molecule level, how accessibility is regulated remains a fundamental question in the field. Here, we use single molecule tracking by high-speed atomic force microscopy to investigate this question using chromatin arrays and extend our findings into the nucleus. By high-speed atomic force microscopy, we tracked chromatin dynamics in real time and observed that the essential kinetochore protein CENP-C reduces the diffusion constant of CENP-A nucleosomes and the linker H1.5 protein restricts H3 nucleosome mobility. We subsequently interrogated how CENP-C modulates CENP-A chromatin dynamics *in vivo*. Overexpressing CENP-C resulted in reduced centromeric transcription and impaired loading of new CENP-A molecules. These data suggest a model in which inner kinetochore proteins are critically involved in modulating chromatin accessibility and consequently, noncoding transcription at human centromeres.

Introduction

Regulating physical access to DNA is central to both gene expression, genome topology, and genome integrity across the eukaryotes. Decades of data from the chromatin transcription field demonstrated that accessible chromatin is more transcriptionally permissive (Klemm et al., 2019; Maeshima et al., 2019; Weintraub and Groudine, 1976; Wu et al., 1979). In contrast, compacted chromatin or heterochromatin is more transcriptionally restrictive (Allshire and Madhani, 2018; Flamm et al., 1969; Janssen et al., 2018; Schultz, 1936). These chromatin states are dynamic and subject to tight regulation. Chromatin-binding proteins dictate many of these dynamics in part

driven by the presence and deposition of specific post-translational modifications (PTMs) of nucleosomes (Rothbart and Strahl, 2014; Taverna et al., 2007; Tolsma and Hansen, 2019). For instance, HP1 binds to H3K9me2/3 nucleosomes (Bannister et al., 2001; Jun-ichi et al., 2001; Lachner et al., 2001; Sanulli et al., 2019a), ultimately resulting in transcriptionally repressive chromatin (Bannister et al., 2001; Escobar et al., 2021; Hwang et al., 2001; Jun-ichi et al., 2001; Lachner et al., 2001). Interestingly, upon binding of HP1 to H3K9me3 nucleosomes, these nucleosomes' internal residues became more exposed to hydrogen/deuterium exchange (Sanulli et al., 2019b). This seminal finding suggests that chromatin-binding proteins not only serve as a recruitment platform for other binding proteins but can rapidly alter the physical properties of individual nucleosomes. The logical extension of this concept is examining how altering innate physical properties of nucleosomes modulates the local chromatin state's structure and function.

In addition to PTMs, the chromatin landscape is also marked by the local enrichment of histone variants (Buschbeck and Hake, 2017; Martire and Banaszynski, 2020; Melters et al., 2015), such as the centromere-specific H3 histone variant CENP-A/CENH3. CENP-A nucleosomes recruit several centromeric proteins (Kai et al., 2021; Mendiburo et al., 2011; Régnier et al., 2005) including CENP-C. CENP-C in turn functions as the blueprint for the formation of the kinetochore (Cheeseman et al., 2006; DeLuca and Musacchio, 2012; Kai et al., 2021; Przewloka et al., 2007; Weir et al., 2016). Recently we reported that a CENP-C fragment (CENP-C^{CD}) induces loss of CENP-C nucleosomal elasticity *in silico* and *in vitro* (Melters et al., 2019). This finding correlates with deceased hydrogen/deuterium exchange of CENP-A nucleosomes when bound by CENP-C (Falk et al., 2016, 2015). Interestingly, when CENP-C was overexpressed, centromeric RNA polymerase 2 (RNAP2) was reduced and centromeric chromatin clustered

together (Melters et al., 2019). We were curious about how CENP-C mechanistically impacts centromeric chromatin fiber accessibility in real time. To address this question, we employed high-speed "video" atomic force microscopy (HS-AFM) to track nucleosomes in arrays over time and extended these findings *in vivo* using immunofluorescence imaging and biochemical approaches. We report that an essential kinetochore protein CENP-C, which is CENP-A chromatin's closest binding partner, directly impacts nucleosome mobility and, surprisingly, also chromatin motions. These data represent a technological advance in imaging and analyzing chromatin dynamics by HS-AFM. Critically, these data provide mechanistic evidence for local transcriptional competency dependent on innate properties and local homeostasis of histone variants within the chromatin fiber.

Results

CENP-C^{CD} represses CENP-A nucleosome mobility *in vitro*

We are interested in understanding how nucleosomes "behave" in biologically relevant conditions. By directly observing nucleosomes using HS-AFM, we were able to assess the motions of individual nucleosomes in real-time. This novel single-molecule technique is powerful, and similar to live cell imaging (Ashwin et al., 2019; Specht et al., 2017) except that nucleosomes can be directly visualized without the need of a fluor-tag. Recently, we showed by HS-AFM that, at the qualitative level, H3 nucleosomes are mobile and make intermittent contact with other H3 nucleosomes (Melters and Dalal, 2021). We therefore set out to quantify the positional dynamics of individual nucleosomes in the context of chromatin by determining the diffusion constant (D) from plots of the mean square displacement (MSD) as a function of time (Figure 1A). Previously, we showed that a fragment of CENP-C rigidified CENP-A nucleosomes

(Melters et al., 2019). Based on these observations, we hypothesized that CENP-C^{CD} would reduce CENP-A nucleosome mobility. To test this hypothesis, we reconstituted CENP-A nucleosomes on a ~3.5 kbp plasmid containing four copies of α-satellite repeats and imaged them by HS-AFM under near physiological conditions. Subsequently, nucleosome tracks were extracted in either the absence (Figure 1B, Supplemental Figure S1, Supplemental movie 1) or presence of CENP-C^{CD} (Figure 1C, Supplemental Figure S1, Supplemental movie 2). The MSD of 134 and 187 tracks, respectively, were calculated (Figure 1D, Supplemental Figure S2A). Individual MSD curves for CENP-A nucleosomes alone were broadly distributed (Supplemental Figure S2A), but the average MSD curve of CENP-A nucleosomes alone reached a steady state after ~60 seconds (Figure 1D), implying confined motion (Kapanidis et al., 2018; Zhong and Wang, 2020).

In contrast, when CENP-C^{CD} was added at 2.2 molar excess to CENP-A nucleosomes (one CENP-C^{CD} molecule per CENP-A molecule), qualitatively CENP-A nucleosome mobility was strongly restricted (Figure 1B). Indeed, the MSD curve was much lower compared to CENP-A alone, and the CENP-C^{CD} MSD curve did not reach a steady state after ~120 seconds. The diffusion constant of CENP-A alone was 10.3±1.5 bp^2/s, whereas the addition of CENP-C^{CD} slowed the diffusion constant by 4-fold to 2.6±0.2 bp^2/s (Figure 1E, Table 1). This difference is reflected in the smaller single frame step-size when CENP-C^{CD} is added to CENP-A chromatin compared to CENP-A chromatin alone (Figure 1F). Looking more closely at the distribution of the average step sizes multiple populations can be inferred, especially in the sample with CENP-C^{CD} (Figure 1G; Supplemental Figure S2). Overall, by HS-AFM we observed that CENP-C^{CD} restricts CENP-A nucleosome mobility. This, we hypothesized could be the mechanism by

which overexpression of CENP-C in living cells results in CENP-A chromatin clustering, as we recently reported (Melters et al., 2019).

H1.5 represses H3 nucleosome mobility *in vitro*

We were curious whether suppression of nucleosome motion by chromatin-binding factors is a shared feature across repressive systems. Thus, we extended this new type of HS-AFM analysis to another factor that is known to repress transcription. A prime candidate is the linker histone H1, which is known to efficiently compact H3 chromatin and restrict transcription (Clausell et al., 2009; Prendergast and Reinberg, 2021; Saha and Dalal, 2021). Previously we published HS-AFM movies of H3 chromatin and H3 chromatin with linker histone variant H1.5 (Melters and Dalal, 2021). Similar as described above, we tracked individual H3 nucleosomes in real-time without (Figure 2A, Supplemental movie 3) and with H1.5 (Figure 2B; Supplemental movie 4) and calculated the MSDs and diffusion constants as described above. H3 nucleosomes alone displayed a broad range of individual MSD curves (Supplemental Figure 3A) and similar to CENP-A alone, the average MSD curve plateaued, implying confined motion (Figure 2C). The diffusion constant for H3 nucleosomes, 21.6±5.1 bp^2/s, was two-fold larger than the diffusion constant for CENP-A (Figure 2D, Table 1).

H1.5 is known to efficiently compact H3 chromatin (Clausell et al., 2009; Prendergast and Reinberg, 2021; Saha and Dalal, 2021). One problem of compacted chromatin is that it impossible to detect and thus track individual nucleosomes. Therefore, we added H1.5 at 0.2 ratio to nucleosomes and measured nucleosome tracks of HS-AFM from which MSDs were calculated. The average MSD curve of H3 chromatin with H1.5 was notably lower than H3

nucleosomes alone (Figure 2C; Supplemental Figure 3). The diffusion constant of H1.5 chromatin was lower (16.7±3.6 bp^2/s) than H3 alone (21.6±5.1 bp^2/s), although this difference was not statistically significant (Figure 2D). The average single step size of the H1.5 sample was shorter than the H3 nucleosomes (Figure 2E) and the distribution of implied multiple populations of diffusing nucleosomes (Figure 2F). One plausible interpretation of these data is that that nucleosome-binding proteins that are associated with chromatin compaction or clustering also mechanistically limit the mobility potential of their cognate nucleosomes.

Excess CENP-C suppresses centromeric chromatin accessibility and transcription *in vivo*

Next, we asked what the functional consequences are of CENP-C on CENP-A chromatin, beyond the formation of kinetochores (Cheeseman et al., 2006; Kai et al., 2021; Mendiburo et al., 2011; Régnier et al., 2005). Previously we showed that overexpressing CENP-C in HeLa cells resulted in increased clustering of centromeric chromatin and loss of centromeric RNAP2 levels (Melters et al., 2019). These results, combined with our "loss of motion" observations above, suggest that centromeric noncoding α-satellite transcription might be impaired in the background of CENP-C over-expression. To examine this facet of CENP-C: CENP-A homeostasis, we overexpressed CENP-C to assess if centromeric transcription is altered.

First, we recapitulated the effects of CENP-C overexpression on the levels of RNAP2 on CENP-A chromatin (Figure 3A, Supplemental Figure S4, two-sided t-test $p<0.05$). In addition, we observed that, upon CENP-C overexpression, total CENP-A levels were reduced (Figure 3B, Supplemental Figure S4; two-sided t-test $p<0.05$). Next, we wondered if CENP-C overexpression impacts centromeric transcription. By quantitative PCR, we observed a ~60%

reduction in α-satellite transcripts in cells overexpressing CENP-C (Figure 3C; two-sided t-test $p<0.01$).

These results indicate that CENP-A levels are reduced and that centromeric transcription is indeed impaired upon CENP-C overexpression. Previous reports showed that new CENP-A loading is transcriptionally regulated (Jansen et al., 2007; Quénet and Dalal, 2014a). Therefore, we hypothesized that CENP-C overexpression leads to defective *de novo* CENP-A loading.

CENP-C overexpression limits *de novo* CENP-A loading

To address this hypothesis, we turned to the well-established SNAP-tagged CENP-A system combined with quench pulse-chase immunofluorescence (Bodor et al., 2012). Using this system in cells synchronized to mid-G1, one can distinguish between older CENP-A (TMR-block) and newly incorporated CENP-A (TMR-Star) (Figures 4A, B). Strikingly, in CENP-C overexpression background we observed a 2.3-fold reduction of *de novo* incorporation of CENP-A (Figures 4C, D, two-sided t-test $p<0.00001$).

Thus, the functional consequences of CENP-C overexpression are suppression of α-satellite transcription (Figure 3C) and impaired CENP-A loading (Figures 4C, D).

Discussion

Here we demonstrate that chromatin accessibility is regulated by modulating nucleosome dynamics through binding of a chromatin effector protein. Specifically, CENP-C^{CD} alone limits the mobility of CENP-A nucleosomes (Figure 1), which correlates with CENP-C^{CD} rigidification

of CENP-A nucleosomes (Melters et al., 2019). CENP-C's capacity to suppress nucleosome mobility was also observed for the linker histone H1.5 (Figure 2). *In vivo*, CENP-C overexpression translates to reduced levels of centromeric RNAP2 (Melters et al., 2019), impaired centromeric transcription (Figure 3C), and subsequent decreased loading of new CENP-A (Figure 4). These findings suggest that physical properties of nucleosomes dictate their mobility along DNA, which in turn regulates chromatin accessibility and transcriptional potential.

Inside the nucleus, nucleosomes move in different dimensions, either in a single dimension along the DNA strand, or two dimensions where the DNA strand moves and the nucleosomes follow as passengers (Babokhov et al., 2020; Melters and Dalal, 2021). In addition, various events, ranging from transcription to DNA repair and replication, involve chromatin remodeling (Nodelman and Bowman, 2021; Zaret, 2020). Several *in vivo* studies have utilized tagged H2B combined with high-resolution live cell imaging to probe nucleosome dynamics. Nucleosomes within heterochromatin were less dynamic compared to euchromatin regions (Nozaki et al., 2017; Ricci et al., 2015) and local levels of H1 correlated with reduced nucleosome dynamics (Gómez-García et al., 2021). Studies using optical tweezers have shown the one dimensional behavior of nucleosomes (Chen et al., 2019; Rudnizky et al., 2019). A recent study showed that the diffusion constant of H3 mononucleosomes sliding along a DNA strand is 0.36 bp^2/s and H2A.Z variant mononucleosomes showed a larger diffusion constant (Rudnizky et al., 2019). Pioneering work by the Lyubchenko lab using HS-AFM showed that CENP-A mononucleosomes are highly mobile (Stumme-Diers et al., 2018). Here, we show that both CENP-A and H3 nucleosomes in the context of chromatin, without being fixed to a surface, have a diffusion constant that is about

30-fold faster (10.3 bp^2/s and 21.6 bp^2/s, respectively). This difference could be due to technical differences of the experimental set-up as well as that our experimental approach allows for both one- and two-dimensional motion of nucleosomes. Interestingly, we observed that the diffusion constant of H3 nucleosomes was two-fold larger compared to CENP-A nucleosomes (Table 1), and H3 nucleosomes are twice as rigid compared to CENP-A nucleosomes (Melters et al., 2019). Looking at another histone variant nucleosome, the diffusion constant of H2A.Z nucleosomes is larger than H3 nucleosomes (Rudnizky et al., 2019), which correlates with the transcriptional buffering function of H2A.Z (Chen et al., 2019; Giaimo et al., 2019). A logical prediction from our results would be that transcription through CENP-A chromatin would be more efficient compared to H3 chromatin.

In contrast, we found that proteins that exert their activity by binding to the outer surface of nucleosomes, rather than changing the make-up of nucleosomes, have the opposite effect on transcription. CENP-C^{CD} rigidifies CENP-A nucleosomes (Melters et al., 2019), but CENP-C^{CD}-CENP-A nucleosomes has a significantly reduced diffusion constant compared to CENP-A nucleosomes alone (Table 1). *In vivo*, overexpression of CENP-C resulted in decreased centromeric transcription (Figure 3C). Similarly, at a H1:nucleosome ratio of 0.2, the linker histone H1.5 also reduced the diffusion of H3 nucleosomes (Table 1). Thus, this study significantly extends the paradigm from the body of work that suggests nucleosome dynamics is a highly tunable platform, with a surprising twist - tuners can dampen or exaggerate nucleosome motions, which correlates with higher order folding.

Taking these and prior findings in context, our data suggest a model where chromatin effector partners modify the material properties of histone variant nucleosomes at the local level, supporting the formation of functional nucleosome clutches (Ricci et al., 2015) (Figure 5). Here we specifically probed CENP-A chromatin and we propose the following model. CENP-A nucleosomes recruit CENP-C which in turn functions as the blueprint for the formation of the kinetochore (Klare et al., 2015). When CENP-C binds, CENP-A nucleosomes become rigidified (Melters et al., 2019) and less mobile (Figure 1), facilitating recruitment of other inner kinetochore components by locally immobilizing CENP-A chromatin. Yet, to load new CENP-A molecules, transcription must happen. The repressive chromatin state that CENP-C induces contradicts this functional necessity. One way cells can work around the juxtaposition of the dual functions of CENP-A chromatin is by maintaining a pool of free centromeric CENP-A nucleosomes in addition to kinetochore-bound CENP-A nucleosomes (Figure 5). Indeed, ChIP-seq and FISH data have established that centromeric CENP-C levels are lower compared to CENP-A levels (Henikoff et al., 2015; Kyriacou and Heun, 2018). We propose that unbound elastic and mobile CENP-A nucleosomes create an intrinsically accessible chromatin state, allowing for the recruitment of the transcriptional machinery to maintain centromeric CENP-A levels to perform both opposing functions. Similarly, H1 variants could create local sites on the chromosome fiber with distinct mechanical states (Figure 5). Succinctly, the epigenetic fate of a locus may be tightly, possibly causally, linked to the mechanical state of the chromatin fiber; concomitantly, the reinstatement of an epigenetic signature by *de novo* loading of a particular variant, reinforces the mechanical state of the fiber.

In summary, in this report we find that CENP-C modulates centromeric chromatin accessibility by directly restricting the motions of CENP-A nucleosomes. *In vivo*, such nucleosome mobility changes correlate with diminished transcriptional competence, resulting in suppression of *de novo* CENP-A loading. Nucleosome dynamics play an important role in genome compaction and regulating DNA access by DNA binding factors. These dynamics are driven by only a few interactions between the interfaces of DNA and nucleosomes (Fierz and Poirier, 2019; Polach and Widom, 1995; Widom, 1998). An exciting line of investigation is to examine how at the nanoscale level the interaction between CENP-A nucleosomes and CENP-C protein co-evolved to repress CENP-A's mobile and elastic nature. It will also be crucial to examine how CENP-A:CENP-C homeostasis, along with those of other key inner kinetochore proteins such as CENP-N, T, S, X, and W regulate centromeric transcription and thereby *de novo* assembly of CENP-A to maintain the epigenetic identity of centromeres in other species. At a more global scale, it will be exciting to ask how different H1 variants modulate the chromatin fiber at the local level to promote or limit transcriptional competency, and how H1 variants dictate the mechanical motions of individual nucleosomes within the local 10nm chromatin fiber.

Material and Methods

Key Resources Table

Reagents or Resource	Source	Identifier	Application	Quantity
ACA serum	BBI Solutions	SG140-2	nChIP	5 µL
Anti-CENP-A (rabbit)	Custom made		nChIP	3 µL
Anti-CENP-A (mouse)	Abcam	ab13939	IF	1:1000
Anti-CENP-A (rabbit)	Abcam	ab45694	WB	1:3000
Anti-CENP-C (guinea pig)	MBL International	PD030	nChIP, IF	5 µL, 1:1000
Anti-CENP-C (rabbit)	Santa Cruz	sc-22789	WB	1:500

Software and Algorithms

Gwyddion	http://gwyddion.net/
R	https://www.r-project.org/
NIH ImageJ	https://imagej.net/software/fiji/
ggplot2	https://cran.r-project.org/web/packages/ggplot2/index.html
CRaQ	http://facilities.igc.gulbenkian.pt/microscopy/microscopy-macros.php
Bio-Formats	https://www.openmicroscopy.org/bio-formats/
Adobe Photoshop	https://www.adobe.com/products/photoshop.html

Native Chromatin-Immunoprecipitation and Western blotting

HeLa cells were grown in DMEM (Invitrogen/ThermoFisher Cat #11965) supplemented with 10% FBS and 1X penicillin and streptomycin cocktail. nChIP experiments were performed without fixation. After cells were grown to ~80% confluency, they were harvested as described (Bui et al., 2017, 2012). For best results, the pellet obtained for chromatin preparation for AFM were spun-down during the nuclei extraction protocol (Walkiewicz et al., 2014) and is broken up with a single gentle tap. Nuclei were digested for 6 minutes with 0.25 U MNase/mL (Sigma-Aldrich cat #N3755-500UN) and supplemented with 1.5 mM $CaCl_2$. Following quenching (10 mM EGTA), nuclei pellets were spun down, and chromatin was extracted gently, overnight in an end-over-end rotator, in low salt solution (0.5X PBS; 0.1 mM EGTA; protease inhibitor cocktail (Roche cat #05056489001). nChIP chromatin bound to Protein G Sepharose beads (GE Healthcare cat #17-0618-02) were gently washed twice with ice cold 0.5X PBS and spun down for 1 minute at 4ºC at 800 rpm. Following the first nChIP, the unbound fraction was used for the sequential nChIP. Western analyses were done using LiCor's Odyssey CLx scanner and Image Studio v2.0.

In vitro reconstition

In vitro reconstitution of CENP-A (CENP-A/H4 cat#16-010 and H2A/H2B cat#15-0311, EpiCypher, Research Triangle Park, NC) and H3 (H3/H4 cat#16-0008 and H2A/H2B cat#15-

0311, EpiCypher Research Triangle Park, NC) nucleosomes were performed as previously described (Dimitriadis et al., 2010; Walkiewicz et al., 2014). For quality purposes, an aliquot of each sample was imaged by AFM in non-contact tapping mode, before moving on to high-speed AFM.

High-speed AFM

In vitro reconstituted CENP-A and H3 chromatin with the addition of CENP-C^{CD} (Melters et al., 2019) or H1.5 (Melters and Dalal, 2021), resp. was imaged with the Cypher VRS (Oxford Instruments, Asylum Research, Santa Barbara, CA) using ultra-small silicon cantilevers (BL-AC10DS with nominal resonances of ~1500 kHz, stiffness of ~0.1 N/m) in non-contact-mode. The mica on top of the scanning pilar was peeled and functionalized with 30 µM APS, before 10 µL of sample was added. The sample was incubated for 15-20 minutes before initializing scanning to obtain a density of ~400 nucleosome/μm^2. The sample was imaged at a speed of 268.82 Hz (frame rate = 1Hz) and a resolution of 512x256 points and lines for an area of 400x400nm (CpA and CpA +CpC^{CD} sample with a nucleosome density of 313 and 394 nucleosomes/μm^2, respectively), 300x300nm (H3 + H1.5 sample with a nucleosome density of 878 nucleosomes/μm^2), and 250x250nm (H3 sample with a nucleosome density of 480 nucleosomes/μm^2). Movies were saved in mp4 format, converted to TIFF sequences using Photoshop (Adobe), and analyzed using manual tracking in ImageJ (Fuji). Obtained nucleosome tracks that were shorter than 10 frames and had single steps exceeding 24 nm were excluded from the analysis. The remaining nucleosome tracks were subsequently analyzed to obtain the mean square displacement curves, diffusion constant, and single frame step sizes; and finally visualized using the ggplot2 package in R (version 4.1.1). The diffusion constant for each

nucleosome sample was estimated from the initial two points of each MSD. The mean and standard error of the mean are reported as the diffusion constant for each nucleosome sample. The mean diffusion constant is identical to the diffusion constant derived from the first two points of the average MSD curves for each nucleosome sample.

Quantitative PCR

α-satellite expression levels in HeLa cells that were either mock transfected or transfected GFP-CENP-C were detected as previously described (McNulty et al., 2017; Quénet and Dalal, 2014b) . RNA was extracted, quantified by UV-spectroscopy, and equal quantities were retro-transcribed using Superscript III First-Strand Synthesis kit as described above. Complementary DNAs (cDNAs) samples were prepared using the iQ SYBR Green supermix (#170–8880; Biorad) following manufacturer's protocol. Control reactions without the cDNA were performed to rule out non-specific amplification. The qtPCR was run on Step one plus Real time PCR system (Applied Biosystem, Grand Island, NY). Primer sequences are:

Oligonucleotides	**Sequence**
Centromeric α-satellite Forward	5'-CATCACAAAGAAGTTTCTGAGAATGCTTC-3'
Centromeric α-satellite Reverse	5'-TGCATTCAACTCACAGAGTTGAACCTTCC-3'
GAPDH Forward	5'-GCGGTTCCGCACATCCCGGTAT-3'
GAPDH Reverse	5'-CCCCACGTCGCAGCTTGCCTA-3'

The comparative cycle threshold (C_T) method was used to analyze the expression level of α-satellite transcripts. C_T values were normalized against the average C_T value of the housekeeping gene GAPDH. Relative fold differences ($2^{-\Delta\Delta CT}$) are indicated in Figure 5C.

Quench pulse-chase immunofluorescence

To quantify *de novo* assembled CENP-A particles, we transfected HeLa cells with SNAP-tagged CENP-A (generous gift from Dan Foltz) in combination with either empty vector or GFP-CENP-C using the Amaxa Nucleofector kit R (Lonza Bioscience, Walkersville, MD) per instructions. The quench pulse-chase experiment was performed according to Bodor et al [42]. In short, following transfection, cells were synchronized with double thymidine block. At the first release TMR-block (S9106S, New England Biolabs, Ipswich, MA) was added per manufactures instruction and incubated for 30 min at 37ºC, followed by three washes with cell culture media. At the second release TMR-Star (S9105S, New England Biolabs, Ipswich, MA) was added per manufactures instructions and incubated for 15 min at 37ºC, followed by three washes with cell culture media. Fourteen hours after adding TMR-Star, cells were fixed with 1% paraformaldehyde in PEM (80 mM K-PIPES pH 6.8, 5 mM EGTA pH 7.0, 2 mM $MgCl_2$) for 10 min at RT. Next, cells were washed the cells three times with ice cold PEM. To extract soluble proteins, cells were incubated with 0.5% Triton-X in CSK (10 mM K-PIPES pH 6.8, 100 mM NaCl, 300 mM sucrose, 3 mM $MgCl_2$, 1 mM EGTA) for 5 min at 4ºC. The cells were rinsed with PEM and fixed for a second time with 4% PFA in PEM for 20 min at 4ºC. Next, the cells were washed three times with PEM. Cells were permeabilized with 0.5% Triton-X in PEM for 5 min at RT and subsequently washes three times with PEM. Next, the cells were incubated in blocking solution (1X PBS, 3% BSA, 5% normal goat serum) for 1 hr at 4ºC. CENP-A antibody (ab13979 1:1000) was added for 1 hr at 4ºC, followed by three washes with 1X PBS-T. Anti-mouse secondary (Alexa-488 1:1000) was added for 1hr at 4ºC, followed by three 1X PBS-T and two 1X PBS washes. Following air-drying, cells were mounted with Vectashield with DAPI (H-1200, Vector Laboratories, Burlingame, CA) and the coverslips were sealed with nail polish. Images were collected using a DeltaVision RT system fitted with a CoolSnap charged-coupled

device camera and mounted on an Olympus IX70. Deconvolved IF images were processed using ImageJ. From up to 22 nuclei, colocalizing CENP-A and TMR-Star foci signal were collected, as well as directly neighboring regions. Background signal intensity was deducted from corresponding CENP-A and TMR-Star signal intensity before the ratio CENP-A/TMR-Star was determined. Graphs were prepared using the ggplot2 package for R.

Quantification and statistical analyses

Significant differences for Western blot quantification and nucleosome track measurements from HS-AFM analyses were performed using either paired or two-sided t-test or one-way ANOVA as described in the figure legends. Significance was determined at $p<0.05$.

Acknowledgements

We thank Drs. Tom Misteli and Sam John, and members of the CSEM laboratory for critical comments and suggestions. We thank Drs. Ankita Saha and Craig Mizzen (deceased, University of Illinois, Urbana-Champaign) for the gift of recombinant H1.5 protein. We thank Dr. Will Heinz for kindly letting us use his custom set-up for HS-AFM. This work was supported by the intramural research fund of the Center for Cancer Research at the National Cancer Institute/NIH (to D.P.M., T.R., and Y.D.) and National Heart, Lung, and Blood Institute (to K.C.N.).

Competing interest: the authors have no competing intertest to declare.

References

Allshire RC, Madhani HD. 2018. Ten principles of heterochromatin formation and function. *Nat*

Rev Mol Cell Biol **19**:229–244. doi:10.1038/nrm.2017.119

Ashwin SS, Nozaki T, Maeshima K, Sasai M. 2019. Organization of fast and slow chromatin revealed by single-nucleosome dynamics. *Proc Natl Acad Sci* **116**:19939 LP – 19944. doi:10.1073/pnas.1907342116

Babokhov M, Hibino K, Itoh Y, Maeshima K. 2020. Local Chromatin Motion and Transcription. *J Mol Biol* **432**:694–700. doi:https://doi.org/10.1016/j.jmb.2019.10.018

Bannister AJ, Zegerman P, Partridge JF, Miska EA, Thomas JO, Allshire RC, Kouzarides T. 2001. Selective recognition of methylated lysine 9 on histone H3 by the HP1 chromo domain. *Nature* **410**:120–124. doi:10.1038/35065138

Bodor DL, Rodríguez MG, Moreno N, Jansen LET. 2012. Analysis of Protein Turnover by Quantitative SNAP-Based Pulse-Chase ImagingCurrent Protocols in Cell Biology. Hoboken, NJ, USA: John Wiley & Sons, Inc. p. Unit8.8. doi:10.1002/0471143030.cb0808s55

Bui M, Dimitriadis EK, Hoischen C, An E, Quénet D, Giebe S, Nita-Lazar A, Diekmann S, Dalal Y. 2012. Cell-Cycle-Dependent Structural Transitions in the Human CENP-A Nucleosome In Vivo. *Cell* **150**:317–326. doi:10.1016/j.cell.2012.05.035

Bui M, Pitman M, Nuccio A, Roque S, Donlin-Asp PG, Nita-Lazar A, Papoian GA, Dalal Y. 2017. Internal modifications in the CENP-A nucleosome modulate centromeric dynamics. *Epigenetics Chromatin* **10**:17. doi:10.1186/s13072-017-0124-6

Buschbeck M, Hake SB. 2017. Variants of core histones and their roles in cell fate decisions, development and cancer. *Nat Rev Mol Cell Biol* **18**:299–314. doi:10.1038/nrm.2016.166

Cheeseman IM, Chappie JS, Wilson-Kubalek EM, Desai A. 2006. The conserved KMN network constitutes the core microtubule-binding site of the kinetochore. *Cell* **127**:983–97.

doi:10.1016/j.cell.2006.09.039

Chen Z, Gabizon R, Brown AI, Lee A, Song A, Celis CD, Kaplan CD, Koslover EF, Yao T, Bustamante C. 2019. High-resolution and high-accuracy topographic and transcriptional maps of the nucleosome barrier. *Elife*. doi:10.7554/eLife.48281

Clausell J, Happel N, Hale TK, Doenecke D, Beato M. 2009. Histone H1 subtypes differentially modulate chromatin condensation without preventing ATP-dependent remodeling by SWI/SNF or NURF. *PLoS One*. doi:10.1371/journal.pone.0007243

DeLuca JG, Musacchio A. 2012. Structural organization of the kinetochore–microtubule interface. *Curr Opin Cell Biol* **24**:48–56. doi:10.1016/j.ceb.2011.11.003

Dimitriadis EK, Weber C, Gill RK, Diekmann S, Dalal Y. 2010. Tetrameric organization of vertebrate centromeric nucleosomes. *Proc Natl Acad Sci U S A* **107**:20317–22. doi:10.1073/pnas.1009563107

Escobar TM, Loyola A, Reinberg D. 2021. Parental nucleosome segregation and the inheritance of cellular identity. *Nat Rev Genet* **22**:379–392. doi:10.1038/s41576-020-00312-w

Falk SJ, Guo LY, Sekulic N, Smoak EM, Mani T, Logsdon GA, Gupta K, Jansen LET, Van Duyne GD, Vinogradov SA, Lampson MA, Black BE. 2015. Chromosomes. CENP-C reshapes and stabilizes CENP-A nucleosomes at the centromere. *Science* **348**:699–703. doi:10.1126/science.1259308

Falk SJ, Lee J, Sekulic N, Sennett MA, Lee T-H, Black BE. 2016. CENP-C directs a structural transition of CENP-A nucleosomes mainly through sliding of DNA gyres. *Nat Struct Mol Biol* **23**:204–208. doi:10.1038/nsmb.3175

Fierz B, Poirier MG. 2019. Biophysics of Chromatin Dynamics. *Annu Rev Biophys* **48**:321–345. doi:10.1146/annurev-biophys-070317-032847

Flamm WG, Walker PMB, McCallum M. 1969. Some properties of the single strands isolated from the DNA of the nuclear satellite of the mouse (Mus musculus). *J Mol Biol* **40**:423–443. doi:https://doi.org/10.1016/0022-2836(69)90163-6

Giaimo BD, Ferrante F, Herchenröther A, Hake SB, Borggrefe T. 2019. The histone variant H2A.Z in gene regulation. *Epigenetics Chromatin* **12**:37. doi:10.1186/s13072-019-0274-9

Gómez-García PA, Portillo-Ledesma S, Neguembor MV, Pesaresi M, Oweis W, Rohrlich T, Wieser S, Meshorer E, Schlick T, Cosma MP, Lakadamyali M. 2021. Mesoscale Modeling and Single-Nucleosome Tracking Reveal Remodeling of Clutch Folding and Dynamics in Stem Cell Differentiation. *Cell Rep* **34**:108614. doi:https://doi.org/10.1016/j.celrep.2020.108614

Henikoff JG, Thakur J, Kasinathan S, Henikoff S. 2015. A unique chromatin complex occupies young α-satellite arrays of human centromeres. *Sci Adv* **1**:e1400234. doi:10.1126/sciadv.1400234

Hwang K-K, Eissenberg JC, Worman HJ. 2001. Transcriptional repression of euchromatic genes by Drosophila heterochromatin protein 1 and histone modifiers. *Proc Natl Acad Sci* **98**:11423 LP – 11427. doi:10.1073/pnas.211303598

Jansen LET, Black BE, Foltz DR, Cleveland DW. 2007. Propagation of centromeric chromatin requires exit from mitosis. *J Cell Biol*. doi:10.1083/jcb.200701066

Janssen A, Colmenares SU, Karpen GH. 2018. Heterochromatin: Guardian of the Genome. *Annu Rev Cell Dev Biol* **34**:265–288. doi:10.1146/annurev-cellbio-100617-062653

Jun-ichi N, C. RJ, D. SB, David AC, S. GSI. 2001. Role of Histone H3 Lysine 9 Methylation in Epigenetic Control of Heterochromatin Assembly. *Science (80-)* **292**:110–113. doi:10.1126/science.1060118

Kai W, Arsen P, Dongqing P, Birte H, Dorothee V, R. VI, Andrea M. 2021. Assembly principles and stoichiometry of a complete human kinetochore module. *Sci Adv* **7**:eabg1037. doi:10.1126/sciadv.abg1037

Kapanidis AN, Uphoff S, Stracy M. 2018. Understanding Protein Mobility in Bacteria by Tracking Single Molecules. *J Mol Biol* **430**:4443–4455. doi:https://doi.org/10.1016/j.jmb.2018.05.002

Klare K, Weir JR, Basilico F, Zimniak T, Massimiliano L, Ludwigs N, Herzog F, Musacchio A. 2015. CENP-C is a blueprint for constitutive centromere-associated network assembly within human kinetochores. *J Cell Biol* **210**:11–22. doi:10.1083/jcb.201412028

Klemm SL, Shipony Z, Greenleaf WJ. 2019. Chromatin accessibility and the regulatory epigenome. *Nat Rev Genet* **20**:207–220. doi:10.1038/s41576-018-0089-8

Kyriacou E, Heun P. 2018. High-resolution mapping of centromeric protein association using APEX-chromatin fibers. *Epigenetics Chromatin* **11**:68. doi:10.1186/s13072-018-0237-6

Lachner M, O'Carroll D, Rea S, Mechtler K, Jenuwein T. 2001. Methylation of histone H3 lysine 9 creates a binding site for HP1 proteins. *Nature* **410**:116–120. doi:10.1038/35065132

Maeshima K, Ide S, Babokhov M. 2019. Dynamic chromatin organization without the 30-nm fiber. *Curr Opin Cell Biol* **58**:95–104. doi:10.1016/j.ceb.2019.02.003

Martire S, Banaszynski LA. 2020. The roles of histone variants in fine-tuning chromatin organization and function. *Nat Rev Mol Cell Biol* **21**:522–541. doi:10.1038/s41580-020-0262-8

McNulty SM, Sullivan LL, Sullivan BA. 2017. Human Centromeres Produce Chromosome-Specific and Array-Specific Alpha Satellite Transcripts that Are Complexed with CENP-A

and CENP-C. *Dev Cell* **42**:226-240.e6. doi:10.1016/j.devcel.2017.07.001

Melters DP, Dalal Y. 2021. Nano-Surveillance: Tracking Individual Molecules in a Sea of Chromatin. *J Mol Biol* **433**:166720. doi:https://doi.org/10.1016/j.jmb.2020.11.019

Melters DP, Nye J, Zhao H, Dalal Y. 2015. Chromatin dynamics in vivo: A game of musical chairs. *Genes (Basel)* **6**. doi:10.3390/genes6030751

Melters DP, Pitman M, Rakshit T, Dimitriadis EK, Bui M, Papoian GA, Dalal Y. 2019. Intrinsic elasticity of nucleosomes is encoded by histone variants and calibrated by their binding partners. *Proc Natl Acad Sci U S A* **116**:24066–24074. doi:10.1073/pnas.1911880116

Mendiburo MJ, Padeken J, Fulop S, Schepers A, Heun P. 2011. Drosophila CENH3 Is Sufficient for Centromere Formation. *Science (80-)* **334**:686–690. doi:10.1126/science.1206880

Nodelman IM, Bowman GD. 2021. Biophysics of Chromatin Remodeling. *Annu Rev Biophys* **50**:73–93. doi:10.1146/annurev-biophys-082520-080201

Nozaki T, Imai R, Tanbo M, Nagashima R, Tamura S, Tani T, Joti Y, Tomita M, Hibino K, Kanemaki MT, Wendt KS, Okada Y, Nagai T, Maeshima K. 2017. Dynamic Organization of Chromatin Domains Revealed by Super-Resolution Live-Cell Imaging. *Mol Cell*. doi:10.1016/j.molcel.2017.06.018

Polach KJ, Widom J. 1995. Mechanism of protein access to specific DNA sequences in chromatin: a dynamic equilibrium model for gene regulation. *J Mol Biol* **254**:130–49. doi:10.1006/jmbi.1995.0606

Prendergast L, Reinberg D. 2021. The missing linker: emerging trends for H1 variant-specific functions. *Genes Dev* **35**:40–58. doi:10.1101/gad.344531.120

Przewloka MR, Zhang W, Costa P, Archambault V, D'Avino PP, Lilley KS, Laue ED, McAinsh AD, Glover DM. 2007. Molecular analysis of core kinetochore composition and assembly

in Drosophila melanogaster. *PLoS One* **2**:e478. doi:10.1371/journal.pone.0000478

Quénet D, Dalal Y. 2014a. A long non-coding RNA is required for targeting centromeric protein A to the human centromere. *Elife* **3**:e03254. doi:10.7554/elife.03254

Quénet D, Dalal Y. 2014b. A long non-coding RNA is required for targeting centromeric protein A to the human centromere. *Elife* **3**:e03254. doi:10.7554/eLife.03254

Régnier V, Vagnarelli P, Fukagawa T, Zerjal T, Burns E, Trouche D, Earnshaw W, Brown W. 2005. CENP-A is required for accurate chromosome segregation and sustained kinetochore association of BubR1. *Mol Cell Biol* **25**:3967–81. doi:10.1128/MCB.25.10.3967-3981.2005

Ricci MA, Manzo C, García-Parajo MF, Lakadamyali M, Cosma MP. 2015. Chromatin Fibers Are Formed by Heterogeneous Groups of Nucleosomes In Vivo. *Cell* **160**:1145–1158. doi:https://doi.org/10.1016/j.cell.2015.01.054

Rothbart SB, Strahl BD. 2014. Interpreting the language of histone and DNA modifications. *Biochim Biophys Acta - Gene Regul Mech*. doi:10.1016/j.bbagrm.2014.03.001

Rudnizky S, Khamis H, Malik O, Melamed P, Kaplan A. 2019. The base pair-scale diffusion of nucleosomes modulates binding of transcription factors. *Proc Natl Acad Sci* **116**:12161 LP – 12166. doi:10.1073/pnas.1815424116

Saha A, Dalal Y. 2021. A glitch in the snitch: the role of linker histone H1 in shaping the epigenome in normal and diseased cells. *Open Biol* **11**:210124. doi:10.1098/rsob.210124

Sanulli S, Trnka MJ, Dharmarajan V, Tibble RW, Pascal BD, Burlingame AL, Griffin PR, Gross JD, Narlikar GJ. 2019a. HP1 reshapes nucleosome core to promote heterochromatin phase separation. *Nature*. doi:10.1038/s41586-019-1669-2

Sanulli S, Trnka MJ, Dharmarajan V, Tibble RW, Pascal BD, Burlingame AL, Griffin PR, Gross JD, Narlikar GJ. 2019b. HP1 reshapes nucleosome core to promote phase separation of

heterochromatin. *Nature*. doi:10.1038/s41586-019-1669-2

Schultz J. 1936. Variegation in Drosophila and the Inert Chromosome Regions. *Proc Natl Acad Sci* **22**:27 LP – 33. doi:10.1073/pnas.22.1.27

Specht EA, Braselmann E, Palmer AE. 2017. A Critical and Comparative Review of Fluorescent Tools for Live-Cell Imaging. *Annu Rev Physiol* **79**:93–117. doi:10.1146/annurev-physiol-022516-034055

Stumme-Diers MP, Banerjee S, Hashemi M, Sun Z, Lyubchenko YL. 2018. Nanoscale dynamics of centromere nucleosomes and the critical roles of CENP-A. *Nucleic Acids Res* **46**:94–103. doi:10.1093/nar/gkx933

Taverna SD, Li H, Ruthenburg AJ, Allis CD, Patel DJ. 2007. How chromatin-binding modules interpret histone modifications: lessons from professional pocket pickers. *Nat Struct Mol Biol* **14**:1025–1040. doi:10.1038/nsmb1338

Tolsma TO, Hansen JC. 2019. Post-translational modifications and chromatin dynamics. *Essays Biochem* **63**:89–96. doi:10.1042/EBC20180067

Walkiewicz MP, Bui M, Quénet D, Dalal Y. 2014. Tracking histone variant nucleosomes across the human cell cycle using biophysical, biochemical, and cytological analyses. *Methods Mol Biol* **1170**:589–615. doi:10.1007/978-1-4939-0888-2_34

Weintraub H, Groudine M. 1976. Chromosomal subunits in active genes have an altered conformation. *Science (80-)*. doi:10.1126/science.948749

Weir JR, Faesen AC, Klare K, Petrovic A, Basilico F, Fischböck J, Pentakota S, Keller J, Pesenti ME, Pan D, Vogt D, Wohlgemuth S, Herzog F, Musacchio A. 2016. Insights from biochemical reconstitution into the architecture of human kinetochores. *Nature* **537**:249–253. doi:10.1038/nature19333

Widom J. 1998. Structure, Dynamics, and Function of Chromatin in vitro. *Annu Rev Biophys Biomol Struct* **27**:285–327. doi:10.1146/annurev.biophys.27.1.285

Wu C, Wong YC, Elgin SCR. 1979. The chromatin structure of specific genes: II. Disruption of chromatin structure during gene activity. *Cell*. doi:10.1016/0092-8674(79)90096-5

Zaret KS. 2020. Pioneer Transcription Factors Initiating Gene Network Changes. *Annu Rev Genet* **54**:367–385. doi:10.1146/annurev-genet-030220-015007

Zhong Y, Wang G. 2020. Three-Dimensional Single Particle Tracking and Its Applications in Confined Environments. *Annu Rev Anal Chem* **13**:381–403. doi:10.1146/annurev-anchem-091819-100409

Table 1. Nucleosome binding proteins slow diffusion constant of target nucleosomes

Sample	*n*	Diffusion constant (nm^2/s)	Diffusion constant (bp^2/s)	Mean step size (nm)
CENP-A nucleosomes	**134**	**1.2±0.2**	**10.3±1.5**	**2.7±0.1**
+ CENP-C^{CD}	**187**	**0.3±0.02**	**2.6±0.2**	**1.9±0.1**
H3 nucleosomes	**24**	**2.6±0.6**	**21.6±5.1**	**3.8±0.4**
+ H1.5	**44**	**1.9±0.4**	**16.7±3.6**	**2.9±0.2**

Either CENP-A or H3 nucleosomes were *in vitro* reconstituted on plasmid DNA and images in fluid in the presence of absence of either 2.2-fold excess CENP-C^{CD} or 0.2-fold excess of H1.5. *n*, number of nucleosomes tracked. For each condition, at least 3 independent replicates were performed.

Figure 1

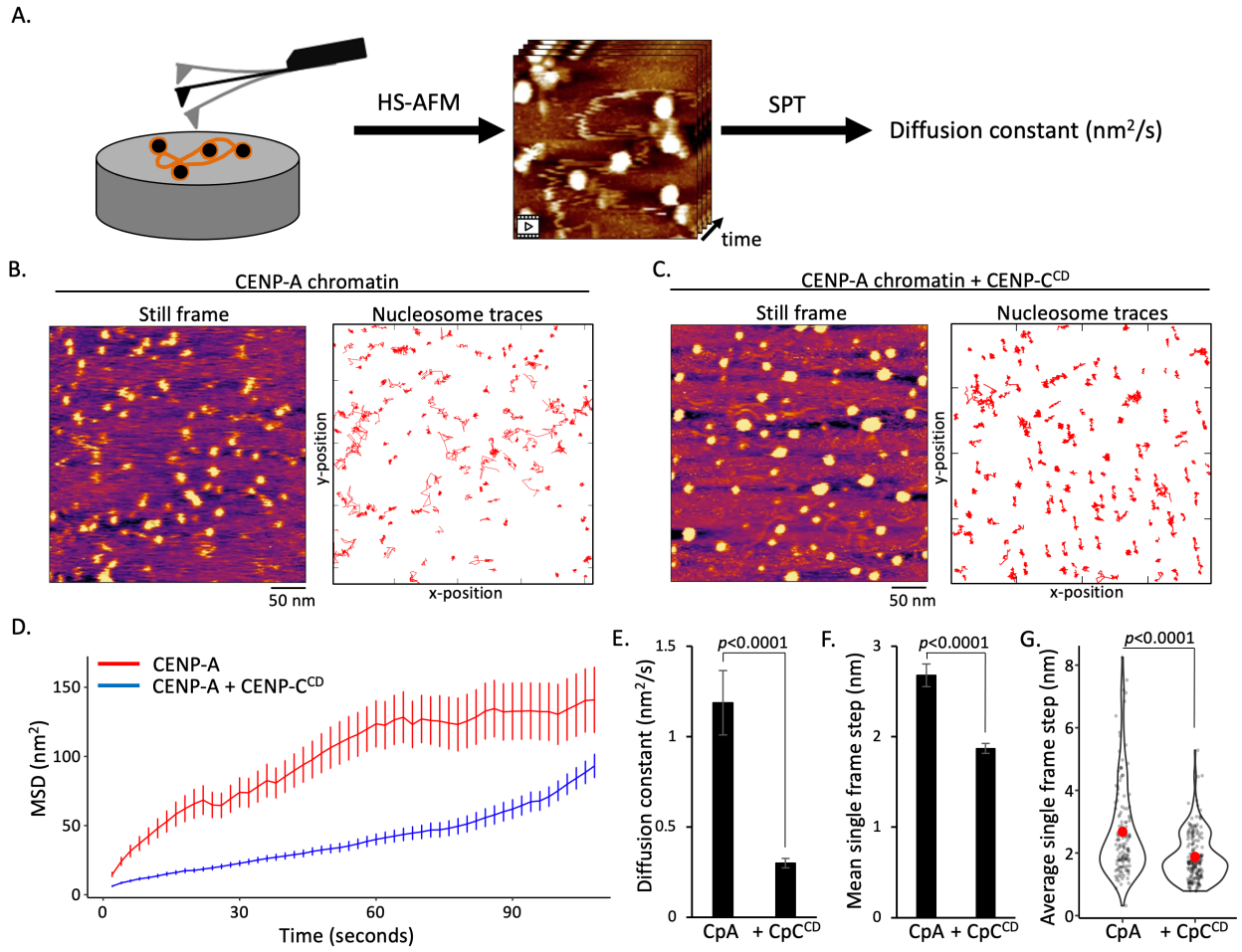

Figure 1. CENP-C^{CD} restrict CENP-A nucleosome mobility *in vitro*
(A) Schematic of experimental set-up. Chromatin was in vitro reconstituted and imaged by HS-AFM in fluid (0.67M NaCl + 2 mM $MgCl_2$) and individual nucleosomes were tracked and analyzed. CENP-A nucleosomes were tracked in fluid for ~120 seconds by HS-AFM at 0.5 Hz alone (B) or in the presence of CENP-C^{CD} (C). Representative images from the movie are shown (B, C), as well as the individual nucleosome trajectories (B, C). (D) The average mean square displacement is shown with standard error as a function of the time interval. (E) The diffusion constants obtained from the MSD curves. (F) The average single frame step-size. (G) The distributions of the average single frame step-sizes for each individual tracked nucleosome (grey points). Red dots represent the overall mean (one-way ANOVA; significance was determined at $p<0.05$).

Figure 2

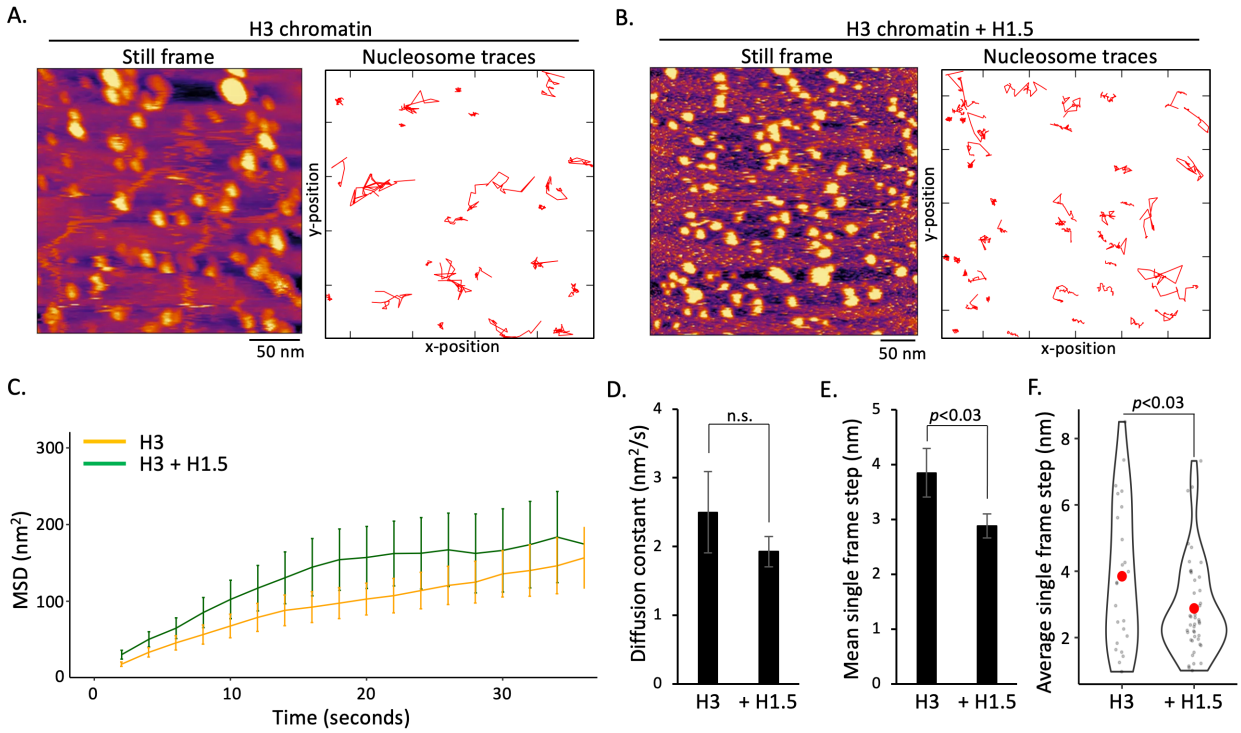

Figure 2. H1.5 restricts H3 nucleosome mobility *in vitro*
H3 nucleosomes were tracked in fluid for ~36 seconds by HS-AFM at 0.5 Hz alone (A) or in the presence of the linker histone H1.5 (B). Representative images from the movie are shown (A, B), as well as the individual nucleosome trajectories (A, B). (C) The average mean square displacement is shown with standard as a function of the time interval. (D) The diffusion constants obtained from the MSD curves. (E) The average single frame step sizes. (F) The distributions of the average single frame step sizes for each individual tracked nucleosome (grey points). Red dots represent the overall mean (two-sided t-test; significance was determined at $p<0.05$).

Figure 3

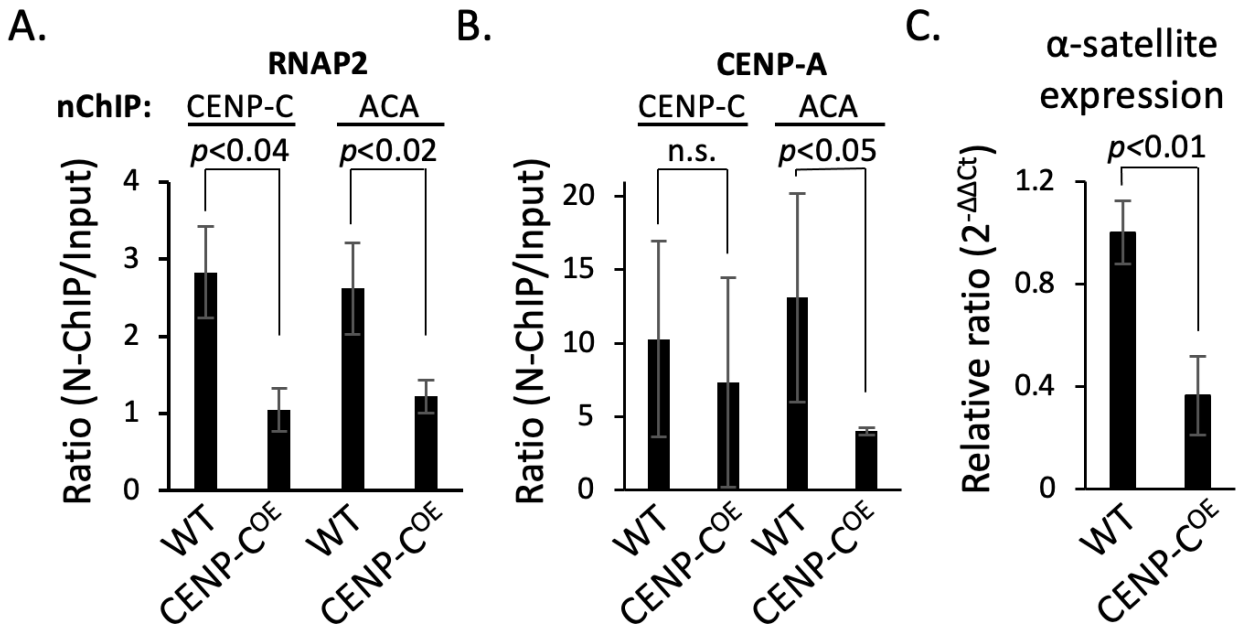

Figure 3. CENP-C overexpression suppressed a-satellite expression and centromeric RNAP2 occupancy
(A) Quantification of RNAP2 levels that pulled down with either CENP-C or sequential ACA nChIP. (B) Quantification of CENP-A levels that pulled down with either CENP-C or sequential ACA nChIP. (C) Quantification of consensus α-satellite transcription in mock-transfected (WT) and CENP-C overexpression (CENP-C^{OE}) (two-sided t-test; significance was determined at $p<0.05$).

Figure 4

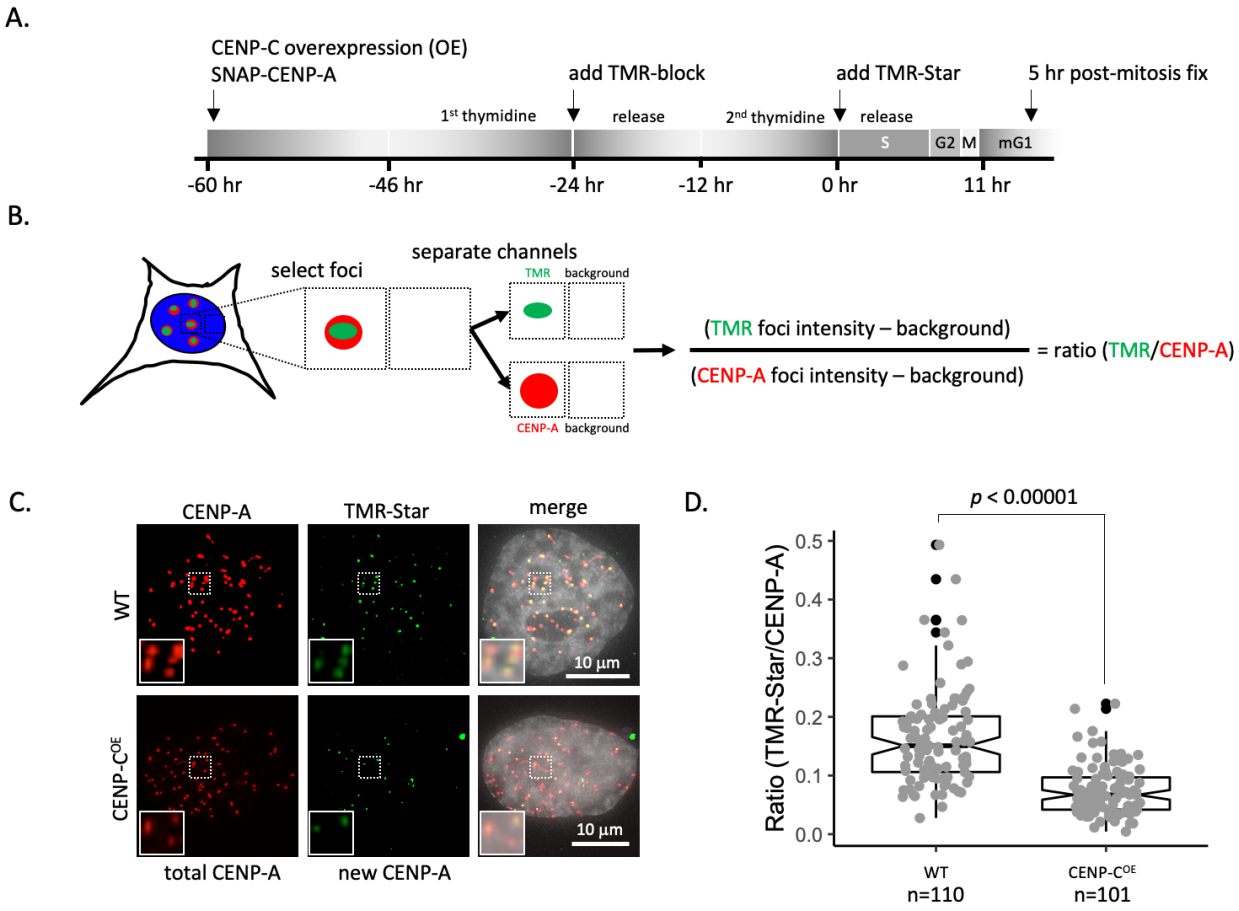

Figure 4. New CENP-A loading impaired upon CENP-C overexpression
(A) Schematic of experimental design. (B) Colocalized immunofluorescent signals for CENP-A and TMR-Star are collected and the intensity of both foci is measured as well as background directly neighboring the foci to determine the ratio of the TMR-star signal over total CENP-A signal. (C) *De novo* CENP-A incorporation was assessed by quench pulse-chase immunofluorescence. After old CENP-A was quenched with TMR-block, newly loaded CENP-A was stained with TMR-Star and foci intensity was measured over total CENP-A foci intensity. Inset is a 2x magnification of the dotted box in each respective image. (D) Quantification of *de novo* CENP-A loading by measuring the ratio of TMR-Star signal over total CENP-A signal (one-way ANOVA; significance was determined at $p<0.05$).

Figure 5

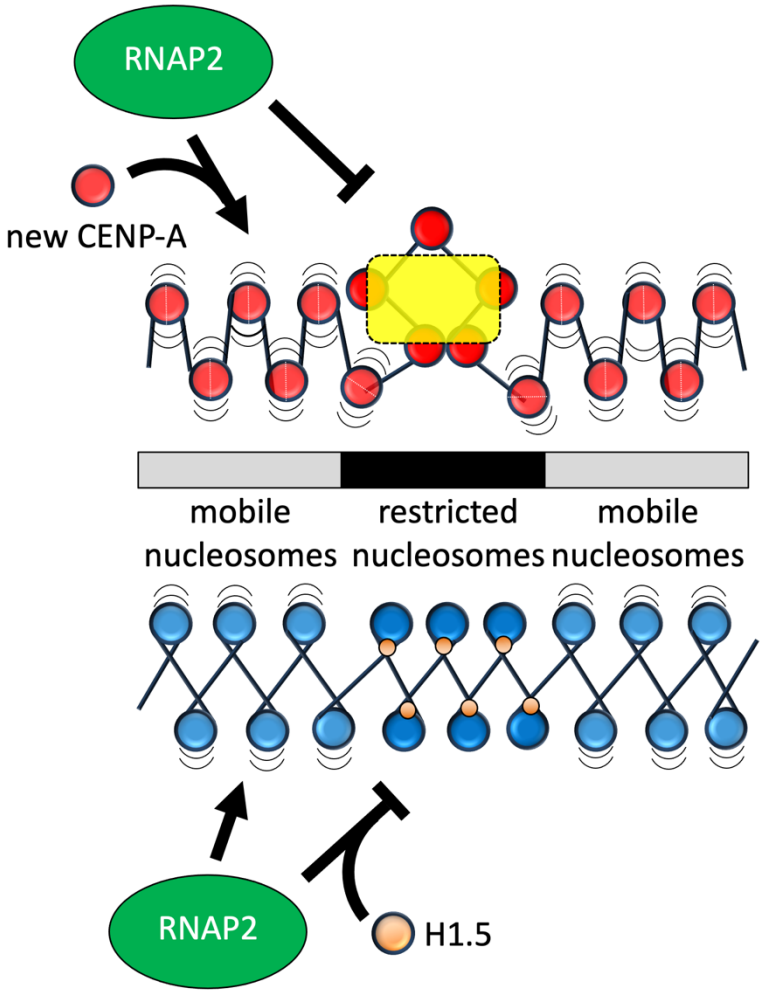

Figure 5. Model of clutches of mobile restricted nucleosomes upon binding of an effector protein. Under wildtype conditions, we propose that CENP-A chromatin not bound by CENP-C (yellow box) and the kinetochore is readily accessible to the transcriptional machinery, because of the intrinsic material properties of CENP-A nucleosomes. In contrast, when CENP-C binds CENP-A nucleosomes, it alters its material properties and quenches CENP-A's mobility resulting in clustered CENP-A chromatin (darker red), restricting progression of the transcriptional machinery and subsequent loading of new CENP-A molecules. Similarly, H1.5 restricts H3 nucleosome mobility (darker blue), impacting RNAP2 transcriptional competency.

SI Appendix, Supplemental Figures

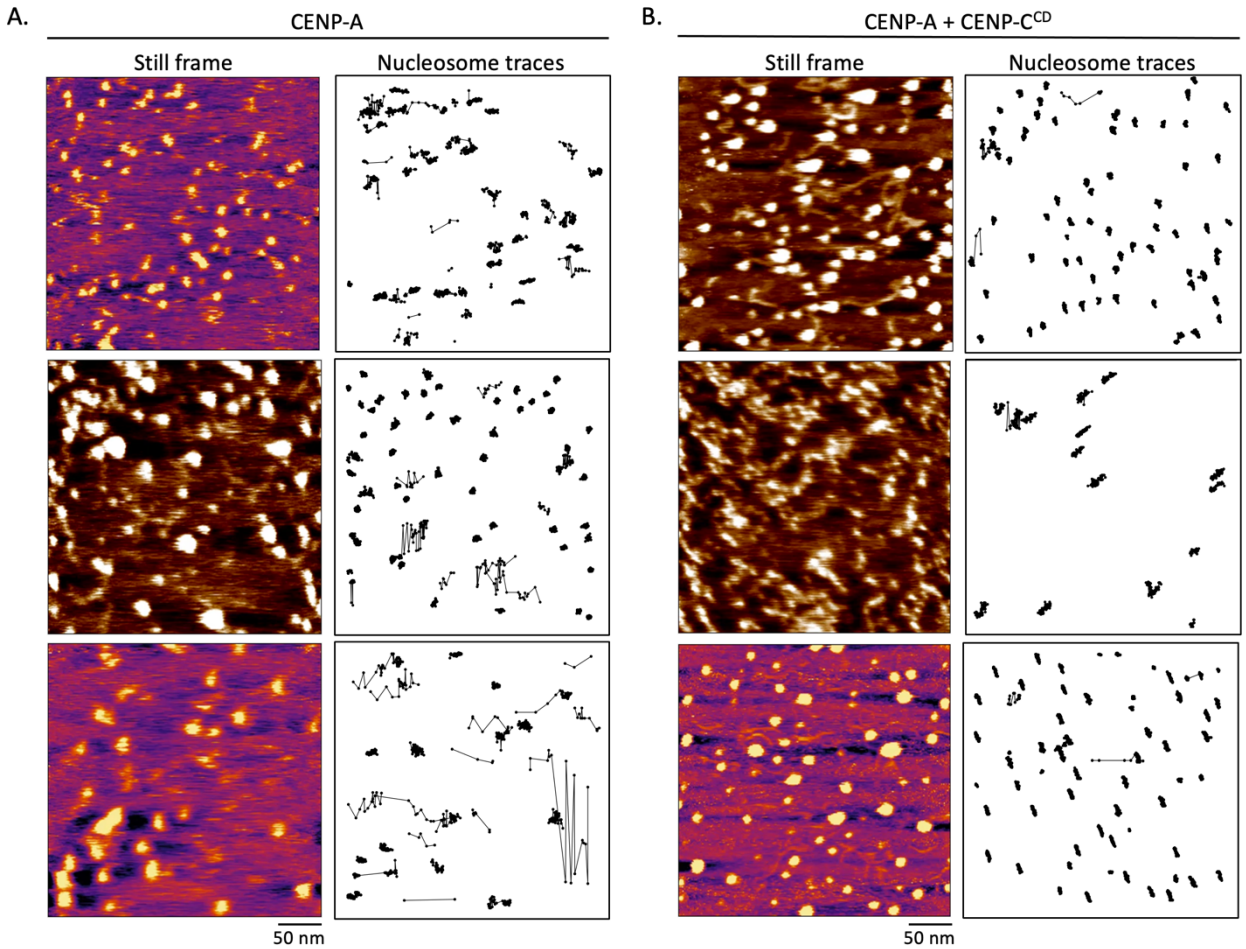

Supplemental Figure 1 – Representative images of three HS-AFM movies and their respective traces for CENP-A alone or CENP-A + CENP-C^{CD}.

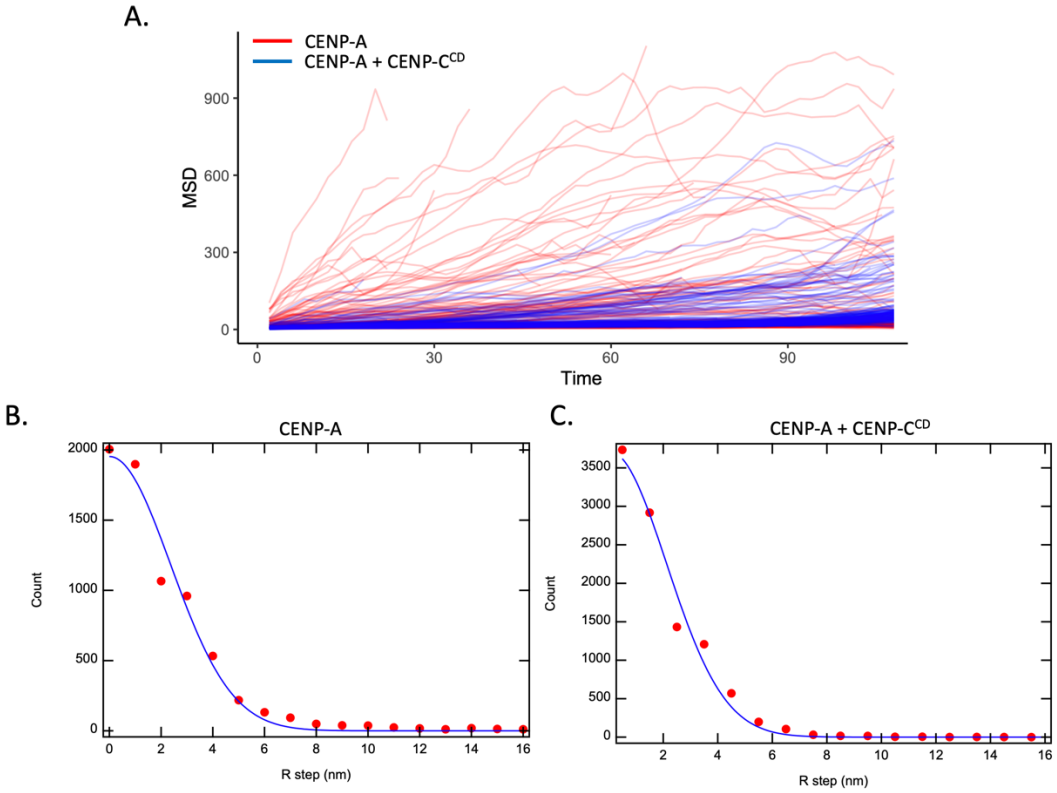

Supplemental Figure 2 – (A) Individual traces for CENP-A and CENP-A + CENP-C^{CD} nucleosomes as summarized in Figure 2 in the main text. (B) and (C) Single step-width was computed for CENP-A alone and CENP-A + CENP-C^{CD} (red dots) and fitted to the predicted step-width from the diffusion constant measured through MSD (blue line).

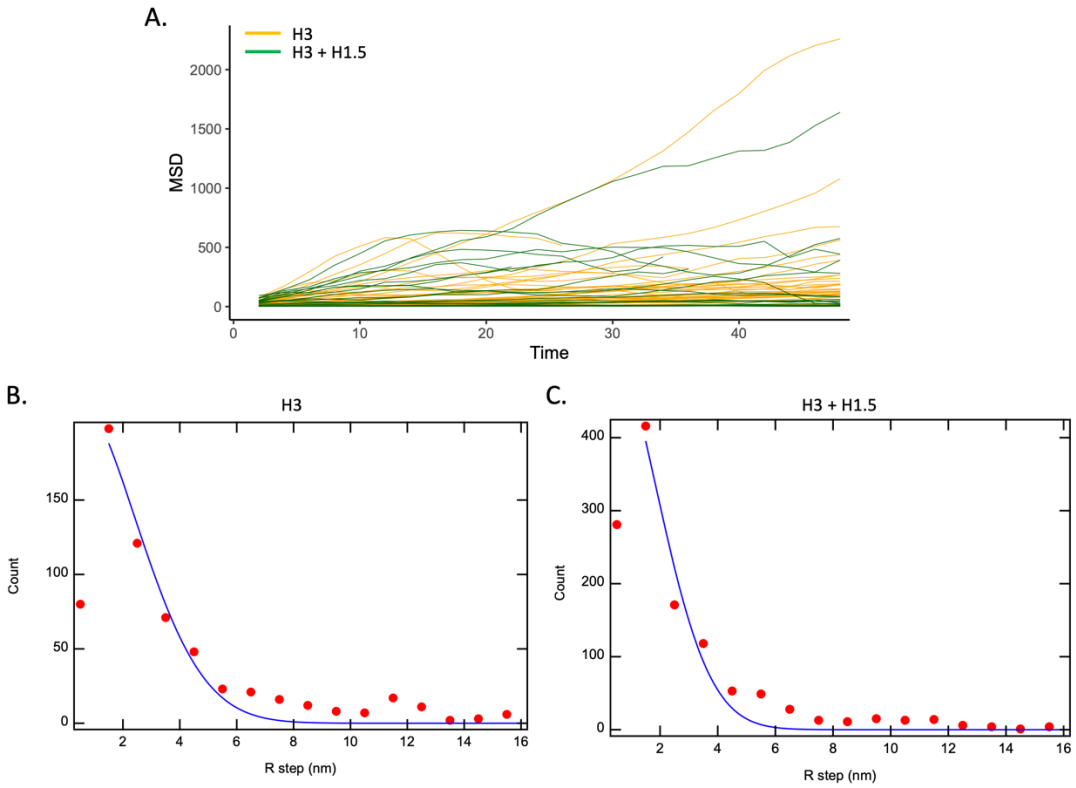

Supplemental Figure 3 – (A) Individual traces for H3 and H3 + H1.5 nucleosomes as summarized in Figure 2 in the main text. (B) and (C) Single step-width was computed for H3 alone and H3 + H1.5 (red dots) and fitted to the predicted step-width from the diffusion constant measured through MSD (blue line).

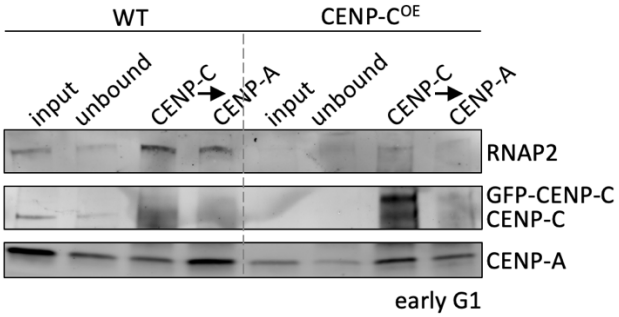

Supplemental Figure 4 – Representative western blot for RNAP2 and CENP-A levels. HeLa cells were transfected with an empty vector (WT) or overexpressing CENP-C (CENP-C^{OE}) and synchronized to early G1 when centromeric transcription is at its highest, similar to what we reported earlier (Melters *et al* 2019 PNAS). We probed for RNAP2, CENP-C, and CENP-A.

Supplemental movie 1 – HS-AFM movie of *in vitro* reconstituted CENP-A chromatin (speed = 2x).

Supplemental movie 2 – HS-AFM movie of in vitro reconstituted CENP-A chromatin with CENP-C^{CD} where CENP-C^{CD} is added at a 2.2x molar ratio to CENP-A nucleosomes (speed = 2x).

Supplemental movie 3 – HS-AFM movie of in vitro reconstituted H3 chromatin (speed = 2x).

Supplemental movie 4 – HS-AFM movie of in vitro reconstituted H3 chromatin with H1.5, where H1.5 is added at a 0.2 molar ratio to H3 nucleosomes (speed = 2x).